A sample of giant radio sources from the NVGRC catalog

O. Zhelenkova[1] · M. Khoruzhenko[2]

[1] Special Astrophysical Observatory of the Russian Academy of Sciences, Nizhny Arkhyz, 369167 Russia
[2] Southern Federal University, Bolshaya Sadovaya st., 105/42, Rostov-on-Don, 344006 Russia

DOI: 10.26119/2025-moc03 EDN: edblkj
eLocator: moc03

Abstract. The NVGRC catalog contains radio sources selected by a pattern recognition algorithm as candidates for giant radio sources (GRSs). Besides genuine GRSs, the catalog includes sources with sizes below 0.7 Mpc and objects erroneously classified as single sources. We examined 370 NVGRC sources along with radio sources located within one degree of the target. The results showed that 48 % of objects are genuine GRSs, 14 % are compact sources with sizes under 0.7 Mpc, and 38 % are misclassified objects. Our study identified 197 giant sources, including 72 previously known GRSs and 125 newly confirmed GRSs. Analysis of the FRItoFRII ratio in the sample revealed nearly equal proportions of these types at $z < 0.05$. At higher redshifts ($z > 0.15$), there is a sharp decrease in the proportion of FRI sources. The predominance of FRII sources in GRS catalogs likely stems from observational selection effects caused by the sensitivity limitations of current radio surveys. Environmental analysis of the GRS sample demonstrated that 39 % have close neighbours within 50 kpc (based on photometric redshifts), 28 % reside in groups or clusters according to published data. When considering radio sources with deformed lobes, nearly 70 % of GRSs appear to be located in relatively dense environments.

Keywords: active galaxies: giant radio sources; general radio continuum

1. Introduction

Giant radio sources are galaxies or quasars, in which the linear size of the radio structure in the projection onto the celestial plane exceeds 0.7 Mpc. The largest known GRSs are approximately 5 Mpc in size, which is comparable to a galaxy cluster. By 2020, approximately 900 GRGs had been discovered (Willis et al. 1974; Lara et al. 2001a; Schoenmakers et al. 2001; Machalski et al. 2001, 2006; Saripalli et al. 2005; Solovyov & Verkhodanov 2014b; Dabhade et al. 2017, 2020; Kuzmicz et al. 2018), and they were considered to be relatively rare objects. Currently, about 12000 GRSs are known (Andernach et al. 2021; Oei et al. 2023; Mostert et al. 2024; Simonte et al. 2024). They were particularly numerous in the coverage area of the LoTSS low-frequency survey, which is characterized by high sensitivity. In other regions of the sky, their detection rate remains relatively low due to the lack of sensitive low-frequency surveys.

There are following hypotheses explaining the size of GRGs. One of them is related to the assumption that the radio source is located in a less dense IGM (InterGalactic Medium), which allows the lobes to expand unhindered (Subrahmanyan et al. 2008; Safouris et al. 2009; Malarecki et al. 2015). Another explanation is the large age of the radio structure, i.e. GRSs are old radio sources (Kaiser et al. 1997). And thirdly, the size is determined by the special properties of the galaxy nucleus, i.e. black hole mass, spin, and accretion rate (Kuzmicz & Jamrozy 2012). It is believed that the GRS is the final phase of the existence of a radio source generated by the galaxy nucleus. Murgia et al. (1999); Parma et al. (1999); Murgia (2003); Jamrozy et al. (2008) have revealed a tendency for the spectral age of radio sources to correlate with linear sizes, i.e. a large age is more often associated with large linear size. However, there also are old radio sources with small sizes that are up to 10^8 years old (Murgia et al. 2011).

Most of the known GRSs are located at close redshifts and are associated with bright elliptical galaxies, classified as FRII type (Fanaroff & Riley 1974) radio sources with radio luminosities in the range of 10^{23}–$10^{28}\mathrm{W}\cdot\mathrm{Hz}^{-1}$ at 1.4 GHz.

GRSs can assist in determining IGM properties. This is due to studies of the interactions of the lobes of radio sources with the environment, detected by the asymmetry of radio structures. Their large size also makes it possible to study the distribution of the warm-hot intergalactic medium in the voids of the large-scale structure of the Universe (Pirya et al. 2012; Malarecki et al. 2015; Peng et al. 2015; Safouris et al. 2009).

Giants transport matter from the host galaxy over long distances and enrich IGM/ISM with non-thermal particles and magnetic fields (Kronberg 1994). This magnetized plasma can exist for billions of years and become a source of injection of high-energy particles into the intracluster medium (Enblin & Gopal-Krishna 2001; van Weeren et al. 2010). GRGs may play an important role in magnetizing the IGM (Oei et al. 2022). The megaparsec-sized radio lobes are the largest natural reservoirs of magnetic field and non-thermal relativistic particles associated with the galactic system, and store most of the energy released by black holes for a very long time (Kronberg et al. 2001). This makes GRSs a good tool for estimating the energy produced by central black holes. The extended GRS lobes with charged particles are large enough to accelerate particles to extremely high energies, and it is assumed that shock waves in radio jets and GRS lobes can generate cosmic rays (Kronberg et al. 2004; Hardcastle et al. 2009).

It was found that the IGM density is quite low in the vicinity of some GRSs (Machalski et al. 2006; Malarecki et al. 2015). Although no association was found between GRSs and voids (Kuzmicz et al. 2018). Moreover, Komberg & Pashchenko (2009) showed that there is no correlation between the size of the radio source and the density of galaxies in its vicinity.

GRGs with sizes $> 4'$ are of particular interest in terms of separating the emission of radio sources from the microwave background, as well as the contribution of sources of different natures to the angular power spectrum used in selecting a cosmological model (Solovyov & Verkhodanov 2014a; Verkhodanov et al. 2016).

Since the IGM density increases as $\rho \propto (1+z)^3$ (Kapahi 1989), the expansion of radio lobes should be difficult at high redshifts. In addition, the surface brightness decreases with redshift as

$(1+z)^{-4}$. This makes it difficult to detect extended radio structures of GRGs in earlier cosmological epochs.

For our work, we used the NVGRC catalog, which was compiled by Proctor (2016). This paper presents a list of GRS-candidates of size $\geq 4''$, selected from the NVSS catalog using pattern recognition algorithms. The identification of host galaxies and determination of their redshifts, which are necessary for determining the projected linear sizes of radio sources, were not carried out in this work. We made a visual inspection of 370 objects, which is about 23 % of the NVGRC catalog. We used all publicly available radio, optical, and infrared surveys to refine the morphology of radio sources and identify host galaxies. A similar study was conducted by Dabhade et al. (2017), where only those NVGRC objects for which a radio core was identified in the VLASS maps were considered. Unlike that publication, we inspected all NVGRC objects, including those for which a radio core was not detected in the VLASS maps.

In this paper, we adopt the ΛCDM flat cosmology based on the Planck results: $H_0 = 67.4\,\mathrm{km\cdot s^{-1}Mpc^{-1}}$, $\Omega_m = 0.315$ (Planck Collaboration 2020). The spectral index of the radio source α is defined as $S_\nu \propto \nu^\alpha$.

2. Search for giant radio sources in the NVGRC catalog

The NVGRC catalog (Proctor 2016) is based on the NVSS (Condon et al. 1998) catalog, in which one radio source can be represented by several entries. To identify giant radio sources, Proctor (2016) used the Oblique Classifier One (OC1) software, which implements the decision tree method (Murthy et al. 1994). The OS1 classifiers were tuned to a training set prepared using the properties of 48 GRGs from Lara et al. (2001a). As a result, a list of 1616 GRS candidates was compiled.

Since radio source identification was not performed, the catalog's sources, in addition to actual giants, include radio sources with smaller projected linear sizes, as well as NVGRC objects in which each of the two components is an independent radio source. For this reason, it is necessary to check each candidate for its classification as a giant.

Next, we describe the methodology we used to recognize giants among the objects in the NVGRC catalog.

2.1. Radio and optical identifications of the candidates

Due to the large angular sizes of GRSs, the identification of their hosts is not an easy task. In addition, if the surface brightness of the radio lobes is low, it is difficult to recognize the GRS itself. If the candidate has a radio core that coincides with the optical object, then the identification is beyond doubt and will be reliable. For radio sources whose core is not detected on the VLASS maps, it is first necessary to recognize the radio structure of the source and determine the position of the host. Optical or ultraviolet radiation hidden by dust structures around the accretion disk of the AGN is re-emitted in the mid-IR range. And in this case, it is the mid-IR data that can help in identifying the host. Data from new radio surveys in the low- and high-frequency ranges help in classifying the radio structure.

Dabhade et al. (2020) conducted a massive search for GRS among NVGRC objects with a radio core in the VLASS maps. We conducted similar work, but, unlike the mentioned paper, we considered objects both with and without a radio core. We also additionally examined one-square-degree neighborhoods for the candidates under consideration.

We used the Aladin Sky Atlas (Bonnarel et al. 2000) and TOPCAT (Taylor 2005) applications to work with numerous catalogs and surveys.

To determine the radio structure of NVGRS objects, we used NVSS, VLASS (Gordon et al. 2021) and FIRST (Helfand et al. 2015)as well as surveys TGSS (Intema et al. 2017), GLEAM (Hurley-Walker et al. 2017), WENSS (Rengelink et al. 1997), SUMSS (Mauch et al. 2003), RACS (McConnell et al. 2020), and in some cases surveys GB6 (Gregory et al. 1996) and Apertif (Rottgering et al. 2011; Adams et al. 2022).

Table 1. The difference in the measured LAS of the giants.

List	N, obj.	$\Delta D \pm$ RMS
K18-D20	257	0.05±0.35
O23-K18	19	0.20±0.28
OL-O23	7	0.18±0.21
OL-D20	51	0.29±0.63
OL-K18	24	0.29±0.18

After the determination of the structure of the radio source, we moved on to optical identification using the surveys SDSS (Ahumada et al. 2020), PanSTARRS (Chambers et al. 2016), DES (Abbott et al. 2018), Legacy Surveys (Dey et al. 2018). If the source did not have a core on the VLASS maps, then the images in the WISE (Cutri et al. 2013) bands were also inspected. If two nearby optical objects were suitable for the role of the host galaxy, then the cutouts from UKIDSS (Lawrence et al. 2007; Lucas et al. 2008) were used. The brighter object in the K-band was considered as a more likely candidate. In addition, we checked the proper motion of the candidate using the GAIA catalog (Gaia Collaboration 2018).

We then searched for spectroscopic or photometric redshifts in the Simbad (Wenger et al. 2000), NED (Helou et al. 1995), NOIR DataLab (Olsen et al. 2019), and Vizier (Ochsenbein et al. 2000) databases.

2.2. Measurment of angular sizes of radio sources

For FR II sources, the angular size is usually measured as the distance between hotspots. For FRI sources and hybrid FRI/FRII objects, the angular size is estimated as the distance between the outer edges of the lobes. In the case of sources that have a strongly curved shape, the angular size is measured along the so-called ridge of the source. Proctor (2016) measured the angular size of the source along the outer edges of the lobes at a level of 3σ above the background level for FRI, FRII, and hybrid types. When measuring, we also did not distinguish between sources of FRI and FRII types. The measurements were performed using the Aladin instrument 'distance'. For sources with curved radio lobes, there is always a certain degree of subjectivity in such measurements.

We measured the angular sizes of the radio sources using VLASS and NVSS cutouts. Some sources on the VLASS maps have only a core and do not even have signs of radio lobes. For them we did not measure the VLASS sizes, and there were 29 such GRS sources. Note, that for 93 of the GRS candidates, the projected linear size obtained from the measurements on the VLASS maps turned out to be less than 0.7 Mpc.

We compared the projected sizes of GRSs that are available in Kuzmicz et al. (2018), Dabhade et al. (2020), Oei et al. (2023) and in our sample. We use for comparison the sizes of radio sources measured by the edges of the source using the NVSS maps. The result can be seen in the Table 1. The first column of the table shows catalogs, for which the difference in the measured angular sizes of the giants is calculated. The designations which are used here: D20 — Dabhade et al. (2020), K18 — Kuzmicz et al. (2018), O23 — Oei et al. (2023) and OL — our list. The second column shows the number of sources that matched in the compared lists. The last column shows the mean difference and the root mean square value in Mpc.

The systematic difference of 0.2–0.3 Mpc between our linear size estimates and the values obtained in Kuzmicz et al. (2018)[1], Dabhade et al. (2020)[2] and Oei et al. (2023) is most likely explained by the fact that we measured the distance not by hot spots, but by the edges of the source.

3. Results of a visual inspection of GRS-candidates

Of the 1616 objects in the NVGRC catalog, we examined 370 (23 %) objects within the right ascension range 00^h00^m < R.A. < 05^h20^m. We also inspected radio sources with angular sizes of 2.5′ and larger, falling into NVSS cutouts with size of one sq. degree centered on the NVGRC object. Some NVGRC objects consist of NVSS components that are physically different radio sources. There are cases when only one component of NVGRC candidate belongs to a radio source classified by us as a GRS. In a number of cases, a GRS not included in the NVGRC was found in the considered NVSS cutouts. Taking into account the aforementioned, 20 GRSs were found that were not included in the NVGRC catalog.

Note that the source J003419.3+011857 in Proctor (2011) is considered as a group of sources, and in Proctor (2016) as a GRS candidate. This object consists of two fairly close radio quasars, as follows from their SDSS DR16 spectroscopic redshifts. The southern source in this pair is classified by Kuzmicz & Jamrozy (2012) as a source whose projected linear size is less than 0.7 Mpc. According to our measurements, and with a redshift higher than what was used in Kuzmicz & Jamrozy (2012), it has size greater than 0.7 Mpc.

Another candidate, J035339.2-011319, was classified as GRG by Dabhade et al. (2020). The radio structure of the northern and southern components of this candidate according to the VLASS maps is more suitable for two double radio sources, and there is definitely an optical identification for the northern component in the PanSTARRS survey. For the southern component, the parent object is a faint optical object in the DECals cutout. We did not consider this source as a giant radio galaxy.

Thus, out of 197 detected GRSs in our sample:

1. 86 GRGs with spectroscopic redshifts. 50 objects are known giant radio galaxies, 36 new GRSs were discovered by us. And six of them are not included in the NVGRC catalog.
2. 72 GRGs with photometric redshifts, 17 objects are included in Dabhade et al. (2020), 55 were discovered by us, and 5 of them are not included in the NVGRC catalog. For 2 of these 5 radio sources, the identification of their hosts turned out to be uncertain due to the complex radio structure. We classified these objects as GRS candidates.
3. Eight GRQs with spectroscopic redshifts. Five are known GRQs, three were discovered by us. And two of them are not included in the NVRSC catalog.
4. Eight quasars with photometric redshifts. They were discovered by us for the first time, and four of them are not included in the NVGSC catalog.
5. 23 parent objects have no redshift information. We consider these objects as candidates.

We could not confidently determine the radio structure of seven NVRGC objects in the catalog J000106.4+340303, J005451.5+564842, J021329.0+292139(2), J025347.1-200007, J032145.1+514855, J035800.3-393629(2), J050341.2-191142. Three NVRGS objects J011352.3+622434, J043503.2+215527, J051219.4+131945 have very weak optical hosts. They are visible only in the PanSTARRS cutouts, but are absent from the PanSTARRS catalog. Their

[1]Our measurements of the angular size for NVGRC J005748.3+302114 differ from Kuzmicz et al. (2018). In our opinion, the northern component of the source bends to the south and is more elongated.

[2]There are differences in the angular sizes for the two sources because we used z that is different from Dabhade et al. (2020). For NVGRC J000622.1+263549, we used z_{ph}=0.835 from the DESI survey instead of z_{ph}=0.436. And for NVGRC J042220.9+151101, we used z_{sp}=0.072 from NED instead of z=0.409.

location relative to the radio structure coincides well with the supposed center of the source. Note that hosts J011352.3+622434 and J051219.4+131945 are in the WISE catalog.

Of the 197 GRSs confirmed by us, 72 sources (68 galaxies and five quasars) are already known from Lara et al. (2001a); Schoenmakers et al. (2001); Kuzmicz & Jamrozy (2012); Kuzmicz et al. (2018); Dabhade et al. (2020); Oei et al. (2023). We found 97 new GRSs (86 GRGs and 11 GRQs) and assigned 28 radio sources to GRS candidates with identified hosts.

Of the 370 considered NVGRC objects, J005748.3+302114 and J010001.3+300249 are a single radio source, as well as J022318.0+425939 and J022251.6+425744, J050533.7-285707 and J050540.8-282445, J051601.7+245826 and J051605.7+245833. Objects J024733.6+615632 and J035322.1+355212 are HII regions.

So out of 370 NVGRC objects, 177 (49 %) were classified as GRSs[3]. The rest of the objects either have sizes less than 0.7 Mpc (13 %), or are physically unrelated radio sources (38 %), which were combined into one system by the recognition algorithm.

The area of the sky that we inspected using the NVGRC cutouts is about 370 sq. degrees. The area of the sky in the range of right ascensions from 00^h00^m to 05^h20^m is about 8600 sq. degrees. Of the 197 GRSs that fell within the surveyed areas, 20 sources were missed by the recognition algorithm and were not included in the NVGRC catalog. Based on this, the estimate of the number of objects missed by the algorithm in this area may be ≈430 objects. Thus, the estimate of the recognition algorithm efficiency is about 30 %. Note that the efficiency of the algorithm Proctor (2016), which is determined by Mostert et al. (2024) from the identifications of candidates with the radio core in Dabhade et al. (2020), is 10 %.

4. Types of parent objects

To classify the bright host objects as quasar/galaxy, we used information available in the Simbad, NED, Vizier, SDSS, and LS databases. Note that in the Simbad and NED databases, it is possible that an optical object is classified as both a galaxy and a quasar. Such a dual type assignment may be due to the appearance of new clarifying information in publications. Also, the host object may belong to "changing-look" AGN (Matt et al. 2000; Denney et al. 2014).

If only photometric data were available for an object, we used the following criteria (Glikman et al. 2018, 2022) based on the color indices using photometry from the AllWISE catalog[4], which are used to select quasars: $0.5 < W1 - W2 < 2$; $2 < W2 - W3 < 4.5$; $W3 - W4 > 1.9$, where W1, W2, W3, W4 are 3.4, 4.6, 12, and 22 μ bands of the Wide-field Infrared Survey Explorer (Wright et al. 2010), respectively.

For weakest hosts, we inspected the WISE cutouts, if an object was bright in the W1 and W2 bands, but was not detected in the W3 and W4 bands, then we attributed it to galaxies. Otherwise, i.e. the object was bright in the W3 and W4 bands, we attributed it to quasars.

As a result, we divided the parent objects into galaxies, quasars, and IR-excess galaxies, whose color indices correspond to the color indices of quasars according to WISE photometry, which amounted to 74 %, 11 %, and 15 %, respectively. For comparison, we note that galaxies among the GRG parent objects account for 82 % in Dabhade et al. (2020) and 80 % in Kuzmicz et al. (2018).

5. Redshifts and radio power

Of the 197 studied radio sources, 94 hosts have spectroscopic redshifts, 80 have photometric redshifts, and for 23 there is no information about redshifts.

[3]This includes GRS-candidates for which we have obtained a redshift estimate or we are not entirely sure about the host identity.

[4]VizieR On-line Data Catalog: II/328.

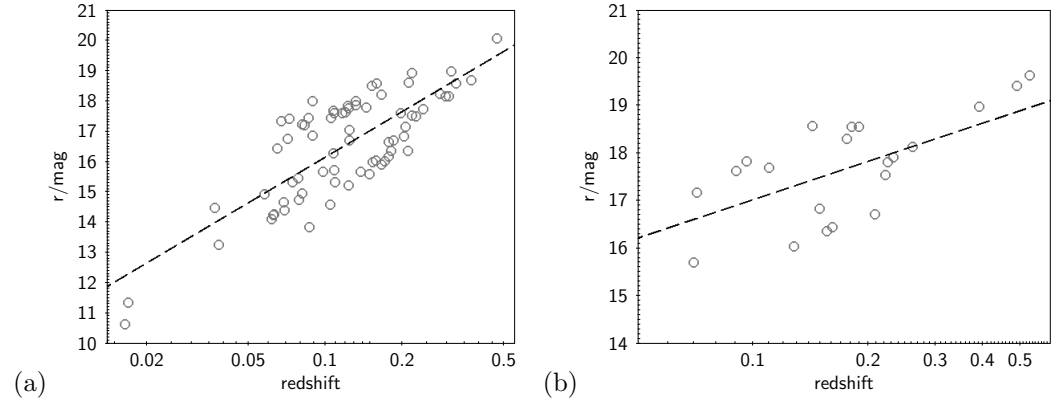

Figure 1. A scatter plot (a) for 71 GRGs with known spectroscopic redshifts and the linear regression (dotted line) between de-reddened apparent r-band magnitudes and spectroscopic redshifts and (b) scatter plot and the regression for 23 GRQs with spectroscopic redshifts. The X-axis is plotted on a logarithmic scale.

5.1. Redshift estimation

Kuzmicz et al. (2018) and Lara et al. (2001b) presented a correlation between the apparent magnitude of GRG hosts and their redshift. This relationship can be used to estimate the "photometric" redshift of galaxies for which redshift data are not available.

Using the r-band apparent magnitude data for GRGs and the spectroscopic redshifts, we constructed a linear regression between these values. The photometric data and spectroscopic redshifts were taken from PanSTARRS, LS and SDSS surveys, NED and SIMBAD databases.

For 71 GRGs the following relationship was obtained (see Fig. 1a):

$$m_r = 5.00 \times \log(z) + 21.16, \tag{1}$$

with a correlation coefficient of $r = 0.78$ and rms = 1.07 mag, where m_r is de-reddened r-band apparent magnitude and z is a spectroscopic redshift.

For GRQ, we constructed a separate dependence. For this, we selected eight quasars and 15 galaxies that can be classified as quasars according to the WISE color indices criterion. The following dependence was obtained (see Fig. 1b):

$$m_r = 2.66 \times \log(z) + 19.69, \tag{2}$$

with a correlation coefficient of $r = 0.72$ and rms = 0.75 mag. These relations were considered for objects with de-reddened magnitudes $m_r < 20.6$. After comparing the spectroscopic redshifts with the values calculated using the obtained formulas, the rms of the difference was about 0.07 for galaxies and 0.15 for quasars.

Using these relationships, we estimated the redshift for 23 parent objects (16 galaxies and 7 quasars), including objects fainter than $m_r = 20.6$. For 94 objects with spectroscopic redshifts, the median value was 0.13; for 80 objects with photometric redshifts — 0.31; for 23 objects with redshift estimates based on the found dependencies, it was 0.63.

5.2. Radio loudness

Relativistic jets, formed as a result of the extraction of the rotational energy of supermassive black holes by a magnetic field and supported by accreting matter, are such effective emitters of radio synchrotron photons that their presence classifies AGNs as members of the class of radio-loud AGN. Now, the classification of AGNs as jetted and non-jetted has become synonymous with the designation of radio-loud and radio-quiet AGNs (Panessa et al. 2019).

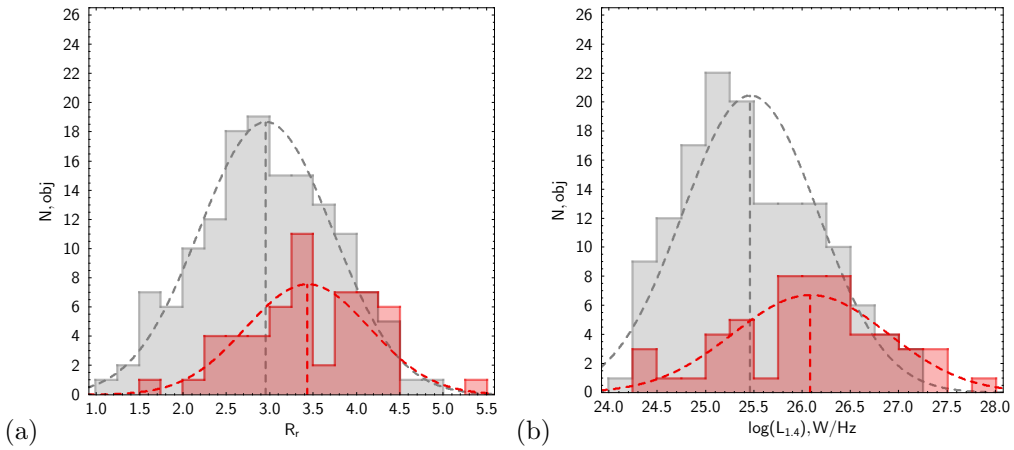

Figure 2. Histograms and their Gaussian fits showing distributions of radio loudness indices (a) and luminosities (b) at 1.4 GHz in W/Hz for galaxies (grey) and quasars and IR-galaxies (red).

To determine radio loudness, we used the approach proposed in the work Ivezic et al. (2002). Here we use the ratio R_r of the radio to optical flux density (without the K-correction) calculated by the formula from Ivezic et al. (2002):

$$R_r = 0.4 \times (m_r - t_N), \tag{3}$$

where m_r is the de-reddened magnitude in the r-band; t_N is the NVSS flux density expressed in the magnitude of the AB-system by the formula:

$$t_N = -2.5 \times \log(F_N/3631\,Jy). \tag{4}$$

Radio sources with $R_r > 1$ are classified as radio-loud AGNs (Kimball & Ivezic 2008). The calculated index values of our list fall within the range from 1.04 to 5.31 (see Fig. 2a), that is, all objects belong to the radio-loud AGNs. The radio loudness index R_r for FRI and FRI/II sources does not exceed 3.5. For FRII sources, it can reach even higher values.

5.3. Radio luminosity

It is known that radio sources can be divided into FRI and FRII depending on morphological type, with the latter being more powerful in the radio band. The radio luminosities of FRI sources at 1.4 GHz lie in the range of 10^{23}–10^{26} W/Hz, of FRII sources — from $10^{24.5}$ W/Hz and higher (Owen & Ledlow 1994). The rest-frame radio power at 1.4 GHz of the sources was estimated using formula from Kuzmicz & Jamrozy (2012):

$$\log L_{1.4} = \log S_{1.4} - (1+\alpha) \times \log(1+z) + 2\log D_l + 17.08, \tag{5}$$

where $S_{1.4}$ is the observed 1.4 GHz flux density (mJy), D_l is the luminosity distance (Mpc), and α is the two-frequency spectral index at 150–1400 MHz, $L_{1.4}$ in W/Hz.

The radio luminosities at 1.4 GHz of the GRSs from our list lie in the range from $10^{24.2}$ to $10^{27.9}$ W/Hz (see Fig. 2b), that is, they all belong to the class of powerful radio sources.

6. Radio morphology

We performed a morphological classification of the giants using cutouts from the NVSS and RACS surveys, as well as cutouts from the FIRST and VLASS surveys with higher angular resolution. Note that the sources under consideration have from 2 to 20 NVSS components.

Table 2. Counts of FRI and FRII sources in redshifts bins

List	z<0.05	0.05÷0.10	0.10÷0.15	0.15÷0.20
D20	4/7	12/29	20/43	6/37
K18	7/5	13/35	10/34	2/32
OL	3/1	13/13	10/26	1/25
mean	52 %	33 %	28 %	9 %

According to the NVSS survey maps, we classified 10 % of the sources as the FRI type, 3 % as the FRI/II type, and 87 % as the FRII type. For Kuzmicz et al. (2018); Dabhade et al. (2020); Andernach et al. (2021), the proportion of FRII sources is 90 %, 89 %, and 93 %, respectively.

We compared the ratio of FRI and FRII sources as a function of redshift for three GRS lists (Dabhade et al. 2020; Kuzmicz et al. 2018; Oei et al. 2023) and our sample. Table 2 presents statistics on the number of FRI, FRI/II, and FRII sources for four redshift intervals. The notations in the list are the same as those in Table 1. In each table cell, the first number indicates the number of FRI and FRI/II sources, and after the slash, the number of FRII sources. The last row of the table shows the average percentage of FRI sources relative to all GRS sources falling in a given redshift interval.

It turns out that at low redshifts ($z < 0.05$) the number of FRI and FRI/II sources can be the same as the number of FRII sources. However, in the redshift interval z=0.15÷0.20, the fraction of FRI sources decreases significantly. Information on the fraction of FRI sources at redshifts $z > 0.2$ is not enough to make estimation. We believe that it is due to the low surface brightness of the outer parts of lobes of FRI sources, GRSs of this type are difficult to detect even at $z > 0.2$. And for this reason, their fraction in the GRS lists is small.

According to VLASS cutouts, we classified 10 % of GRSs as sources with a core-jet/core-lobes morphology, 17 % of the objects as double sources, 57 % of the sources as doubles with a core, and 16 % of the sources as triples[5]. Thus, it turned out that 83 % of the sources on the VLASS cutouts have a radio core, which makes it possible to identify hosts reliably.

Deformation, curvature of the lobes of a radio source is an indicator of its environment and/or processes occurring in the immediate vicinity of the AGN. So, tailed morphology (WAT, Wide-Angle Tailed or NAT, Narrow-Angle Tailed) indicates that the source can be located in clusters or groups of galaxies (Owen & Rudnick 1976; Missaglia et al. 2019). In 22 % of the giants, we noted HT (Head-Tail) features.

A X-, Z-, S-shaped morphology of the radiolobes is explained by a change in the orientation of the jets, either due to the merger of a small galaxy with the massive elliptical host, or due to accretion disk instabilities (Dennett-Thorpe et al. 2002; Liu 2004; Joshi et al. 2019).

Sources that show double-double morphology (Brocksopp et al. 2011) as well as triple morphology (Gopal-Krishna et al. 2012) are classified as AGN with radiophase restart. We combined S-, Z-, X- sources with double-double and triple sources, since their morphological features indicate processes occurring close to the active nucleus. In 26 % of the sources, it is possible to detect such features in the radiolobes.

Some of the GRGs from our sample exhibit a combination of the aforementioned morphological features. Thus, approximately half of the sources exhibited additional features of the morphology of the radio lobes.

Comparing the NVSS and VLASS cutouts, we found that some sources have radio lobes at 1.4 GHz, but they are absent or weakly expressed on 3 GHz maps. In our list of GRSs, such sources turned out to be 38 %.

[5]We refer to triple sources as those in which the integrated core flux density can be 10–20 % of the total flux of the source at the NVSS, RACS, or TGSS catalogs.

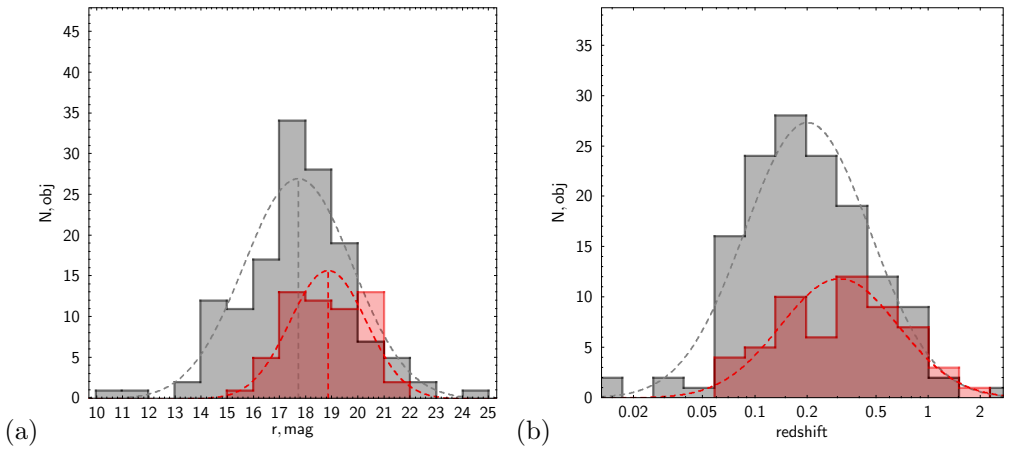

Figure 3. The histograms and their Gaussian fits show the distribution of de-redded magnitudes in the r band (a) and redshifts in logarithmic scale (b) of hosts for 140 GRSs with neighbors (gray) and 57 GRSs without neighbors (red).

If we take into account the occurrence of weakly pronounced lobes on the VLASS maps, then such feature occurs in 13–14 % of quasars and galaxies with an IR excess, and in 40 % of normal galaxies.

7. Environment of giant radio sources

When examining the environment of the GRGs, we considered the presence of optical neighbors and deformation of radio lobes, and also searched for indications of the host belonging to a group or cluster of galaxies in publications. During a detailed visual inspection of the giant hosts' surroundings using cutouts from optical surveys, we noted the presence of neighbors within the distance of approximately 50 kpc, which is between $1''$ and $2'$ depending on the redshift.

We divided the GRSs into groups, ranging from those with no signs of a nearby environment to those with confirmed membership in a group or cluster of galaxies as reported in the publications. No neighbors were found near 36 hosts, and for 21 hosts there is no information about the redshifts of their neighbors. The remaining hosts have neighbors with redshifts matching the hosts' redshifts within the measurement error, and/or the radio source has S-, Z-, or X-shaped morphology, and/or it belongs to a group or cluster of galaxies, and/or the giant has a head-tail morphology. As a result, we found that 140 (71 %) of the objects in our GRS list have close neighbors confirmed by redshift or radio lobe morphology and/or are members of galaxy groups or clusters.

Figure 3 shows the histograms showing the magnitude (a) and redshift (b) distributions for GRSs with neighbors (light grey) and GRSs without neighbors marked with a red line.

The median values of apparent r-band magnitudes and redshifts for host galaxies with confirmed neighbors and host galaxies without neighbors are $18^m.1$ and 0.19, $19^m.3$ and 0.31, respectively. Thus, host galaxies for which we did not find neighbors are fainter and more distant than those for which the neighbors are confirmed. We believe that these differences are partly explained by observational selection. It can be assumed that the number of host galaxies with neighbors may exceed 70 %.

8. Conclusions

We examined objects from the NVGRC catalog in the interval $00^h00^m < R.A. < 05^h20^m$ in order to search for giant radio sources. Of the 370 objects, 48 % were classified as giant radio

sources, 14 % had sizes smaller than 0.72 Mpc, and 38 % were independent radio sources combined into one system by the recognition algorithm. When examining NVSS cutouts of one sq. degree, centered on the NVGRC object, 20 giants were detected that are absent from the catalog. Taking this into account, we estimated the efficiency of the recognition algorithm (Proctor 2016) to be approximately 30 %.

Of the 197 GRSs we discovered, 72 sources (68 galaxies and five quasars) are already known in the catalogs Lara et al. (2001a); Schoenmakers et al. (2001); Kuzmicz & Jamrozy (2012); Kuzmicz et al. (2018); Dabhade et al. (2020). We discovered 97 new giants (86 BRKs and 11 quasars) for which spectroscopic or photometric redshifts are known for their hosts. For another 28 GRSs, the redshifts were estimated using the $m_r - z$ relation.

After studying the NVSS cutouts, we classified 87 % of the sources as FRII. It should be noted that the proportion of FRII sources was approximately the same as in Kuzmicz et al. (2018); Dabhade et al. (2020); Andernach et al. (2021) — 90 %, 92 %, and 93 %, respectively. We compared the proportion of FRI giants by selecting sources in four redshift bins. For $z < 0.05$, the proportion of FRI and FRII sources was approximately equal, but already for $z > 0.15$, the proportion of FRI giants sharply decreases. Thus, the predominance of FRII type giants in the GRS lists is most likely associated with observational selection due to the sensitivity limit of existing radio surveys.

According to VLASS maps, 83 % of the sources exhibit core-jet, core-lobe, double-core, or triple morphology. Thus, it turned out that 83 % of the giants have a radio core, which makes it possible to reliably identify hosts.

Comparing the NVSS and VLASS cutouts, we found that 33 % of sources can be classified as "faded". 25 % of the sources show a restart of the radio source phase. 38 % of the sources have deformed radio lobes.

With the help of parent objects with spectroscopic redshifts, relationships between apparent magnitudes and redshifts were determined, which were used to estimate redshifts for 28 GRSs without redshift data.

When determining the type of the parent object, we mainly used information from the Simbad and NED databases. For those objects for which we did not have this information, we applied the criteria that separate galaxies and quasars according to the WISE photometry. This was mainly used for faint objects. As a result, our GRG sample includes 74 % of galaxies, 15 % of IR-excess galaxies, which, according to the WISE photometric data, can be attributed to quasars, and 11 % of quasars.

When inspecting optical survey maps, we noted close neighbors and the association of host galaxies with groups or clusters of galaxies, taking into account radio morphology and, of course, information from publications. It turned out that close neighbors were found in 140 of the radio sources. Thus, 71 % of GRGs are in a fairly dense environment, and this fraction may be higher.

The area of the sky in the range of right ascensions from 00^h00^m to 05^h20^m is 8600 sq. degrees. Of which, we examined 370 sq. degrees. Of the 197 GRS sources that fell within the examined areas, 20 were missed by the recognition algorithm and are not included in the NVGRC catalog. Based on this, the estimate of the number of objects missed by the algorithm in this area may be ≈ 430 objects. Thus, the estimate of the efficiency of the recognition algorithm is about 30 %.

Acknowledgements This research uses services or data provided by the Astro Data Lab at NSF's NOIRLab. NOIRLab is operated by the Association of Universities for Research in Astronomy (AURA), Inc. under a cooperative agreement with the National Science Foundation; This research has made use of the NASA/IPAC Extragalactic Database, which is funded by the National Aeronautics and Space Administration and operated by the California Institute of Technology; the CATS database, available on the Special Astrophysical Observatory website.

Funding

The work was carried out within the framework of the state assignment of SAO RAS, approved by the Ministry of Science and Higher Education of the Russian Federation.

References

Abbott T., Abdalla F., Allam S., et al., 2018, Astrophysical Journal Suppl., 239, 2, id. 18
Adams E., Adebahr B., de Blok W., et al., 2022, Astronomy and Astrophysics, 667, id. A38
Ahumada R., Allende P., Almeida A., et al., 2020, Astrophysical Journal Suppl., 249, 1, id. 3
Andernach H., Jimenez-Andrade E., Willis A., 2021, Galaxies, 9, 4, id. 99
Bonnarel F., Fernique P., Bienayme O., et al., 2000, Astronomy and Astrophysics Suppl., 143, p. 33
Brocksopp C., Kaiser C., Schoenmakers A., et al., 2011, Monthly Notices of the Royal Astronomical Society, 410, 1, p. 484
Chambers K.C., Magnier E.A., Metcalfe N., et al., 2016, eprint arXiv:1612.05560
Condon J., Cotton W., Greisen E., et al., 1998, Astronomical Journal, 115, 5, p. 1693
Cutri R., Wright E., Conrow T., et al., 2013, Explanatory Suppl. to the AllWISE DR Products
Dabhade P., Gaikwad M., Bagchi J., et al., 2017, Monthly Notices of the Royal Astronomical Society, 469, 3, p. 2886
Dabhade P., Mahato M., Bagchi J., et al., 2020, Astronomy and Astrophysics, 642, id. A153
Dennett-Thorpe J., Scheuer P., Laing R., et al., 2002, Monthly Notices of the Royal Astronomical Society, 330, 3, p. 609
Denney K., De Rosa G., Croxall K., et al., 2014, Astrophysical Journal, 796, 2, id. 134
Dey A., Schlegel D., Lang D., et al., 2018, Astronomical Journal, 157, 5, id. 168
Enblin T. and Gopal-Krishna, 2001, ASP Conference Series, 250, p. 454
Fanaroff B. and Riley J., 1974, Monthly Notices of the Royal Astronomical Society, 167, p. 31
Gaia Collaboration, Brown A., Vallenari A., et al., 2018, Astronomy and Astrophysics, 616, id.A1
Glikman E., Lacy M., LaMassa S., et al., 2018, Astrophysical Journal, 861, 1, id. 37
Glikman E., Lacy M., LaMassa S., et al., 2022, Astrophysical Journal, 934, 2, id. 119
Gopal-Krishna, Biermann P., Gergely L., et al., 2012, Research in Astronomy and Astrophysics, 12, 2, p. 127
Gordon Y., Boyce M., O'Dea C., et al., 2021, Astrophysical Journal Suppl., 255, 2, id.30
Gregory P., Scott W., Douglas K., et al., 1996, Astrophysical Journal Suppl., 103, p. 427
Hardcastle M., Cheung C., Feain I., et al., 2009, Monthly Notices of the Royal Astronomical Society, 393, 3, p. 1041
Helfand D., White R., Becker R., 2015, Astrophysical Journal, 801, 1, id. 26
Helou G.; Madore B.F.; Schmitz M., et al., 1995, Astrophysics and Space Science Library, 203, p.95
Hurley-Walker N., Callingham J., Hancock P., et al., 2017, Monthly Notices of the Royal Astronomical Society, 464, 1, p. 1146
Intema H., Jagannathan P., Mooley K., et al., 2017, Astronomy and Astrophysics, 598, id. A78
Ivezic Z., Menou K., Knapp G., et al., 2002, Astronomical Journal, 124, 5, p. 2364
Jamrozy M., Konar C., Machalski J., et al., 2008, Monthly Notices of the Royal Astronomical Society, 385, 3, p. 1286
Joshi R., Krishna G., Yang X., et al., 2019, Astrophysical Journal, 887, 2, id. 266
Kaiser C., Dennett-Thorpe J., Alexander P., 1997, Monthly Notices of the Royal Astronomical Society, 292, 3, p. 723
Kapahi V., 1989, Astronomical Journal, 97, p. 1
Kimball A. and Ivezic Z., 2008, Astronomical Journal, 136, 2, p. 684
Komberg B. and Pashchenko I., 2009, Astronomy Reports, 53, 12, p.1086
Kronberg P., 1994, Reports on Progress in Physics, 57, 4, p. 325
Kronberg P., Dufton Q., Li H., et al., 2001, Astrophysical Journal, 560, 1, p. 178
Kronberg P., Colgate S., Li H., et al., 2004, Astrophysical Journal, 604, 2, p. L77
Kuzmicz A. and Jamrozy M., 2012, Monthly Notices of the Royal Astronomical Society, 426, 2, p. 851
Kuzmicz A., Jamrozy M., Bronarska K., et al., 2018, Astrophysical Journal Suppl., 238, 1, id. 9
Lara L., Cotton W., Feretti L., et al., 2001, Astronomy and Astrophysics, 370, p. 409
Lara L., Márquez I., Cotton W., et al., 2001, Astronomy and Astrophysics, 378, p. 826
Lawrence A., Warren S., Almaini O., et al., 2007, Monthly Notices of the Royal Astronomical Society, 379, 4, p. 1599
Liu F., 2004, Monthly Notices of the Royal Astronomical Society, 347, 4, p. 1357
Lucas P., Hoare M., Longmore A., et al., 2008, Monthly Notices of the Royal Astronomical Society, 391, 1, p. 136
Machalski J., Jamrozy M., Zola S., 2001, Astronomy and Astrophysics, 371, p. 445
Machalski J., Jamrozy, M., Zola, S., et al., 2006, Astronomy and Astrophysics, 454, 1, p. 85
Malarecki J., Jones D., Saripalli L., et al., 2015, Monthly Notices of the Royal Astronomical Society, 449, 1, p. 955
Matt G., Guainazzi M., Maiolino R., 2000, Monthly Notice of the Royal Astronomical Society, 342, 2, p. 422
Mauch T., Murphy T., Buttery H., et al., 2003, Monthly Notice of the Royal Astronomical Society, 342, 4, p. 1117
McConnell D., Hale C., Lenc, E., et al., 2020, Publications of the Astronomical Society of Australia, 37, id. E048
Missaglia V., Massaro F., Capetti A., et al., 2019, Astronomy and Astrophysics, 626, id. A8
Mostert R., Oei M., Barkus B., et al., 2024, Astronomy and Astrophysics, 691, id. A185
Murgia M., Fanti C., Fanti R., et al., 1999, Astronomy and Astrophysics, 345, p. 769
Murgia M., 2003, Publications of the Astronomical Society of Australia, 20, 1, p. 19
Murgia M., Parma P., Mack K., 2011, Astronomy and Astrophysics, 526, id. A148
Murthy S., Kasif S., Salzberg S., 1994, arXiv e-prints, cs/9408103
Ochsenbein F., Bauer P., Marcout J., 2000, Astronomy and Astrophysics Suppl., 143, p. 23
Oei M., van Weeren R., Hardcastle M., et al., 2022, Astronomy and Astrophysics, 660, id. A2

Oei M., van Weeren R., Gast A., et al., 2023, Astronomy and Astrophysics, 672, id. A163
Olsen K., Bolton A., Juneau S., et al., 2019, Bulletin of the American Astronomical Society, 51, 7, id. 61
Owen F. and Ledlow M., 1994, ASP Conf. Ser., 54, p. 319
Owen F. and Rudnick L., 1976, Astrophysical Journal Letters, 205, p. L1
Panessa F., Baldi R., Laor A., et al., 2019, Nature Astronomy, 3, p. 387
Parma P., Murgia M., Morganti R., et al., 1999, Astronomy and Astrophysics, 344, p. 7
Peng B., Chen R., Strom R., 2015, Proc. of AASKA14, Online at http://pos.sissa.it/cgi-bin/reader/conf.cgi?confid=215, id.109
Pirya A., Saikia D., Singh M., et al., 2012, Monthly Notices of the Royal Astronomical Society, 426, 1, p. 758
Planck Collaboration, 2020, Astronomy and Astrophysics, 641, id. A6
Proctor D., 2011, Astrophysical Journal Suppl., 194, 2, id. 31
Proctor D., 2016, Astrophysical Journal Suppl., 224, 2, id. 18
Rengelink R., Tang Y., de Bruyn A., et al., 1997, Astronomy and Astrophysics Suppl., 124, p. 259
Rottgering H., Afonso J., Barthel P., et al., 2011, Journal of Astrophysics and Astronomy, 32, 4, p. 557
Safouris V., Subrahmanyan R., Bicknell G., et al., 2009, Monthly Notices of the Royal Astronomical Society, 393, 1, p. 2
Saripalli L., Hunstead R., Subrahmanyan R., et al., 2005, Astronomical Journal, 130, 3, p. 896
Schoenmakers A., de Bruyn A., Rottgering H., et al., 2001, Astronomy and Astrophysics, 374, p. 861
Simonte M., Andernach H., Bruggen M., et al., 2024, Astronomy and Astrophysics, 686, id. A21
Solovyov D. and Verkhodanov O., 2014, Astronomy Reports, 58, 8, p. 506
Solovyov D. and Verkhodanov O., 2014, Astrophysical Bulletin, 69, 2, p. 141
Subrahmanyan R., Saripalli L., Safouris V., et al., 2008, ASP Conf. Ser., 395, p. 380
Taylor M., 2005, ADASS XIV, ASP Conf. Ser, 347, p. 29
van Weeren R., Rottgering H., Bruggen M., et al., 2010, Science, 330, 6002, p. 347
Verkhodanov O., Solovyov D., Ulakhovich O., et al., 2016, Astrophysical Bulletin, 71, 2, p. 139
Wenger M., Ochsenbein F., Egret D., et al., 2000, Astronomy and Astrophysics Suppl., 143, p. 9
Willis A., Strom R., Wilson A., 1974, Nature, 250, 5468, p. 625
Wright E., Eisenhardt P., Mainzer A., et al., 2010, Astronomical Journal, 140, 6, pp. 1868